

Fragment Binding to β -Secretase 1 without Catalytic Aspartate Interactions Identified via Orthogonal Screening Approaches

Frederik J. R. Rombouts,^{*,†} Richard Alexander,^{||} Erna Cleiren,[‡] Alex De Groot,[‡] Michel Carpentier,[‡] Joyce Dijkmans,[‡] Katleen Fierens,[‡] Stefan Masure,[‡] Diederik Moechars,[§] Martina Palomino-Schätzlein,[⊥] Antonio Pineda-Lucena,^{⊥,∇} Andrés A. Trabanco,[#] Daan Van Glabbeek,[‡] Ann Vos,[‡] and Gary Tresadern[‡]

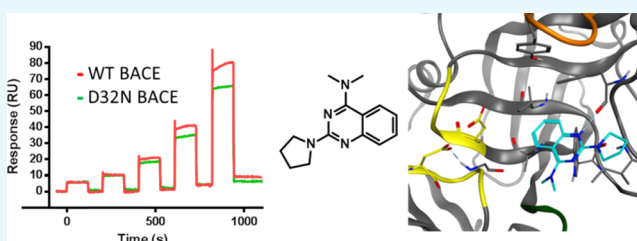
[†]Neuroscience Medicinal Chemistry, [‡]Discovery Sciences, and [§]Neuroscience Biology, Janssen Research & Development, Turnhoutseweg 30, B-2340 Beerse, Belgium

^{||}Discovery Sciences, Janssen Research & Development, 1400 McKean Road, Spring House, Pennsylvania 19477, United States

[⊥]Structural Biochemistry Laboratory, Centro de Investigación Príncipe Felipe, Eduardo Primo Yúfera, 3, 46012 Valencia, Spain

[#]Neuroscience Medicinal Chemistry, Janssen Research & Development, C/ Jarama 75A, 45007 Toledo, Spain

ABSTRACT: An approach to identify β -secretase 1 (BACE1) fragment binders that do not interact with the catalytic aspartate dyad is presented. A ThermoFluor (thermal shift) and a fluorescence resonance energy transfer enzymatic screen on the soluble domain of BACE1, together with a surface plasmon resonance (SPR) screen on the soluble domain of BACE1 and a mutant of one catalytic Asp (D32N), were run in parallel. Fragments that were active in at least two of these assays were further confirmed using one-dimensional NMR (WaterLOGSY) and SPR binding competition studies with peptidic inhibitor OM99-2. Protein-observed NMR (two-dimensional ¹⁵N heteronuclear single-quantum coherence spectroscopy) and crystallographic studies with the soluble domain of BACE1 identified a unique and novel binding mode for compound **12**, a fragment that still occupies the active site while not making any interactions with catalytic Asps. This novel approach of combining orthogonal fragment screening techniques, for both wild-type and mutant enzymes, as well as binding competition studies could be generalized to other targets to overcome undesired interaction motifs and as a hit-generation approach in highly constrained intellectual property space.



INTRODUCTION

Alzheimer's disease (AD) is a neurodegenerative disorder and a massive societal burden.^{1,2} Available treatments only provide a modest delay of the cognitive decline.³ Considerable research efforts aim to intervene in disease progression.^{4–6} Among these, inhibition of β -secretase 1 (BACE1) is the most studied since its discovery in 1999.^{7–10} The approach prevents the cleavage of the amyloid precursor protein (APP) into neurotoxic $A\beta_{40-42}$ peptide products, which aggregate to form the extracellular amyloid plaques found in the AD brains.¹¹ Genetic evidence also supports BACE1 as a target for AD.¹²

BACE1 is a membrane-anchored aspartic protease with three domains: an N-terminal ectodomain, a single transmembrane domain, and a cytosolic C-terminus. The catalytic ectodomain has an aspartic protease fold, with the substrate-binding cleft located between the N- and C-terminal lobes (Figure 1). The crucial catalytic aspartate (Asp) dyad, D32 and D228, is located at the interface of the two lobes.⁷ A hairpin loop “flap” in the N-terminal lobe partially covers the cleft in a perpendicular orientation. The conformational changes in the flap control the substrate access to the active site, and open to closed conformations have been observed in crystal structures of

BACE1.^{13,14} Loops C, D, and F in the C-lobe of the ectodomain are the epitopes for binding of a known antibody.¹⁵

The first BACE1 inhibitors were substrate analogues that mimicked the APP-cleavage sequence with a noncleavable peptide bond. They displayed high in vitro potency but typically had poor oral bioavailability and low brain penetration.^{16–18} The discovery of amidine moieties that form optimal interactions with the Asp dyad revolutionized the field of BACE1 inhibitors, as improved drug likeness became possible.¹⁹ These Asp-binding amidine and guanidine motifs have been widely explored (Chart 1A),¹⁹ including studies conducted in our labs (compounds **1**, **3**, and **4**).^{20–25} Compound **1** was reported to bend back, allowing the distal *N*-cyclohexyl group to occupy the S1 pocket, whereas the central cyclohexyl occupied the lipophilic S1' pocket. Compounds **2** and **3** on the other hand contain a quaternary sp³ carbon, which provides an ideal vector into the S1–S3 and S2' pockets of the catalytic site (Figure 1).²⁶ Although a step forward, the basicity of the amidine/guanidine function provides a formal positive

Received: December 8, 2016

Accepted: February 10, 2017

Published: February 24, 2017

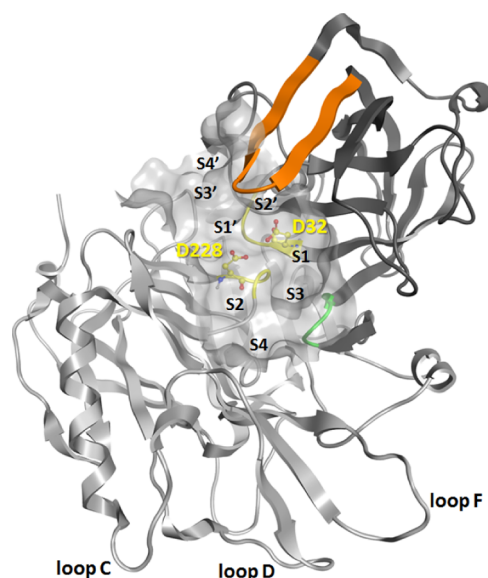


Figure 1. BACE1 (PDB 1XN3) in ribbon representation with the N-terminal lobe in dark gray, C-terminal lobe in light gray, active site with the catalytic Asp dyad in yellow, flap in orange, and 10S loop in green. The substrate-binding cleft is shown as a surface together with the location of subpockets S1, S2, S3, S4, S1', S2', S3', and S4'.

charge, impacting the optimization of physicochemical parameters. In contrast, there are a few known ligands that bind to the catalytic cleft without interacting with the Asp dyad. Pyrimidine **6** was reported by Merck to bind to the S1 and S3 pockets²⁷ (Chart 1B), and dihydroisoquinolines **7** and **8** were reported by Elan Pharmaceuticals^{28–30} to bind to the S2 pocket. Hence, the drawbacks of amidine inhibitors and the limited intellectual property (IP) space spurred our interest to seek alternatives to binding at the Asp dyad.

Fragment-based drug discovery has now become an accepted strategy for hit finding in drug discovery.^{31,32} The principle is that structurally smaller “fragment-like” hits (generally MW below 250 D or ~21 heavy atoms) can be evolved into more optimal binders with superior properties than those of traditional high-throughput screen (HTS) hits. Because of their few but optimal interactions, fragment hits typically have low affinity in the high micromolar or low millimolar range. Hence, fragment screens are often performed at similar concentration ranges using sensitive biophysical techniques, such as surface plasmon resonance (SPR), ThermoFluor (TF), ligand-observed NMR, and sometimes X-ray screening. Although normally the throughput is lower than that of biochemical HTS assays, the fragment space is exponentially smaller, requiring only thousands of fragments to cover a similar chemistry space, than that in HTS decks of hundreds of thousands of compounds.³³ Fragments are more likely progressed to leads when the activity is confirmed by orthogonal screening techniques, and also knowing the binding mode via crystallography can be crucial to improve potency. Numerous BACE1 leads have evolved from fragment screening,³⁴ most binding to the catalytic Asp dyad, for instance those from Edwards et al. (Chart 1, compound **2**).²⁴ Hence, fragment screening can be successful, but careful consideration is needed to overcome the contemporary challenges of BACE1 inhibition. Here, we applied orthogonal screening approaches, leading to the identification of a non-Asp-binding fragment, for which a

crystal structure was obtained showing a distinct and previously undescribed binding mode.

RESULTS AND DISCUSSION

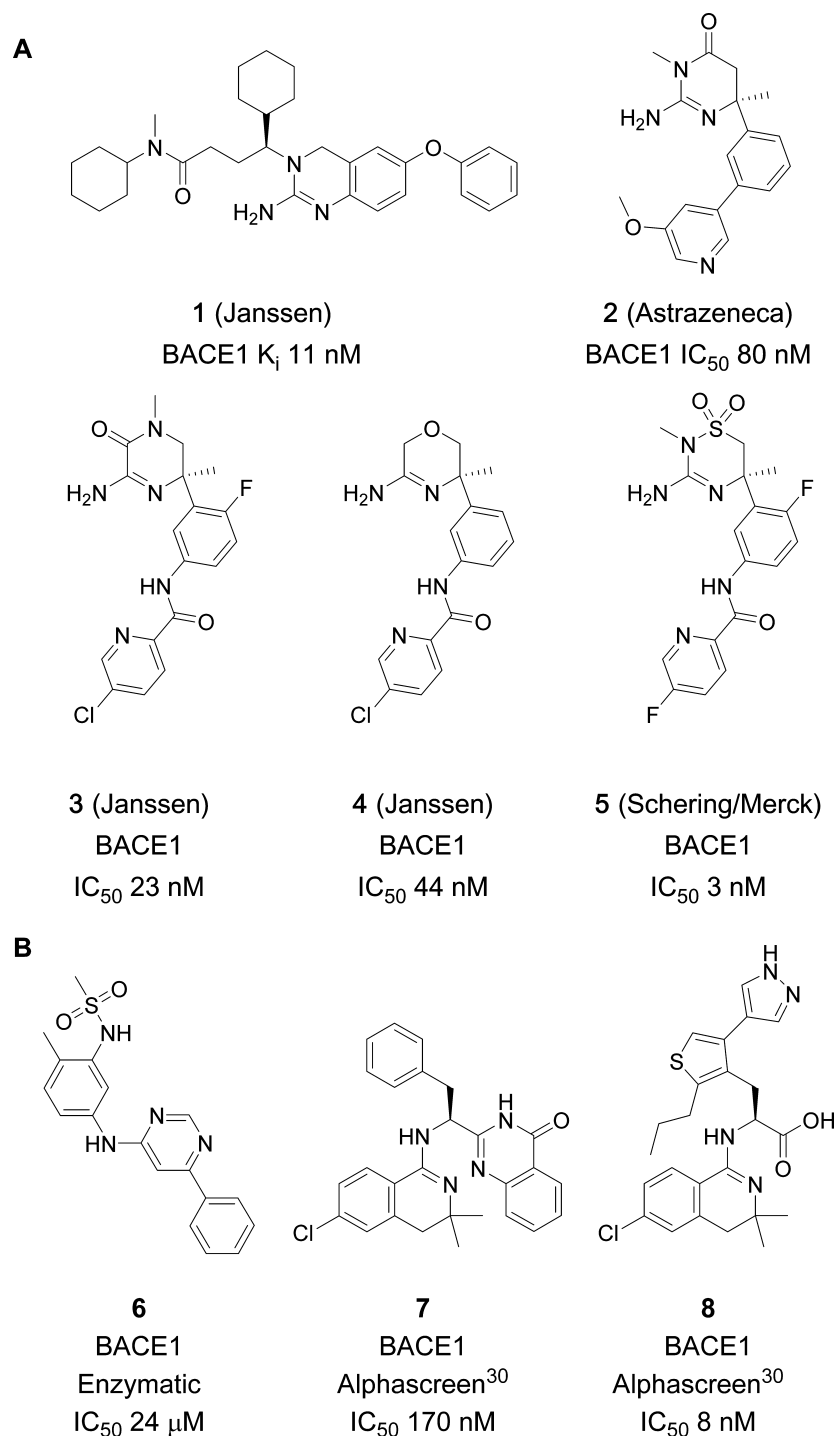
Overview of the Approach. We defined a strategy to identify the fragments that do not interact with the catalytic Asps, Figure 2. An SPR screen of the Janssen Fragment Library (JFL) was conducted at two pH values using the Biacore 4000 system with the mature BACE1 ectodomain and neutravidin (reference protein) immobilized. In parallel, TF and enzymatic FRET assays were run at high compound concentration. These allowed additional triage and permitted us to identify false positives from the SPR screen. The hits were further characterized in a new SPR screen by assessing their binding in the presence of the potent peptidomimetic inhibitor, OM99-2 (FRET IC_{50} , 4.38 nM; SPR K_{d} , 12.7 nM),³⁵ known to occupy most subpockets of wild-type (WT) BACE1 and the active-site mutant D32N. This approach provided additional information on the binding site and discriminated only the most promising fragments. Hits with an attractive structure and desired binding profile were then confirmed by WaterLOGSY,³⁶ and the actives were submitted to protein-observed ¹H–¹⁵N TROSY NMR and/or X-ray crystallography.³⁷

Fragment Library. High-concentration screens often render assays sensitive to false positives resulting from minor impurities in the screening samples.³⁸ Janssen R&D has therefore invested in a fragment collection in which all compounds have been analyzed by LC/MS with UV or CLND detection and their dimethyl sulfoxide (DMSO) solutions have been analyzed for structure plausibility by NMR using the Bruker CMC-Q software. The purity threshold in LC/MS and NMR was set to 95% and above. Fragments with 8–21 heavy atoms were selected from both our screening deck and internally synthesized intermediates or final compounds. These were stored in 100, 50, or 20 mM DMSO solutions depending on the solubility. The library was constructed on the basis of criteria such as 2D shape, 2D fingerprint, and scaffold diversity. Similarities to both the known drugs and the number of sp³ centers were also promoted in the selection process. The size of the JFL used in this study was 1120 compounds.

SPR Screen. For SPR-based fragment screening, the mature BACE1 ectodomain was immobilized on a CM7 sensor chip together with neutravidin (reference). First, all fragments were tested for promiscuous binding, that is, showing nonspecific interaction with the target and/or reference protein, resulting in high baseline increase or decrease, or showing irregular sensorgram shapes. Nine fragments were removed from the JFL due to promiscuous binding. Next, the JFL was screened in duplicate using a compound concentration of 0.25 mM at both pHs 7.4 and 4.5 because Dominguez et al. demonstrated that BACE1 inhibitors binding well at acidic and neutral pH values could be optimal cellular inhibitors as they maintain interaction with BACE1 throughout the transport from the neutral extracellular environment through to the acidic endosome.³⁹ Concentration-reponse (CR) curves were subsequently generated for hits at either pH value or both pH values.

TF Screen. Thermal shift analysis of the mature BACE1 ectodomain was used to estimate binding affinities by measuring the effect of a ligand on protein stability using thermal denaturation.^{40,41} The JFL was tested in duplicate at a single concentration (2.1, 0.8, or 0.2 mM based on the respective haystack DMSO concentration of 100, 50, or 20

Chart 1. (A) Examples of Amidine-Based BACE1 Inhibitors Reported by AstraZeneca, Janssen, and Schering/Merck; (B) Examples of Orthosteric Non-Asp BACE1 Binders



mM). Fragments showing a significant ΔT_m shift compared to the average protein-only control value were confirmed by CR curves.

Enzymatic Screen. BACE1 enzymatic activity was assessed by a FRET assay using a mature BACE1 ectodomain. An APP-derived 13 amino acid substrate containing the “Swedish” Lys-Met/Asn-Leu mutation at the cleavage site was employed. 7-Methoxycoumarin-4-yl acetic acid (MCA) was the fluorescent donor, and 2,4-dinitrophenyl (DNP) was the acceptor. The 100, 50, and 20 mM haystack samples of the JFL were first

screened at 33.3-fold dilution, hence at 3.0, 1.5, and 0.6 mM, respectively. Hits with $\geq 49\%$ inhibition were subsequently tested twice by CR curves. Autofluorescent compounds (sample at T_0 minus mean control at $T_0 > 3 \times \sigma$) were removed.

SPR Competition and Mutant BACE1 Experiments. To identify fragment binding in the vicinity of the Asp’s, a competition between OM99-2 and the mature BACE1 ectodomain was performed with six overlapping hits from the prior assays. In addition, SPR binding experiments versus the

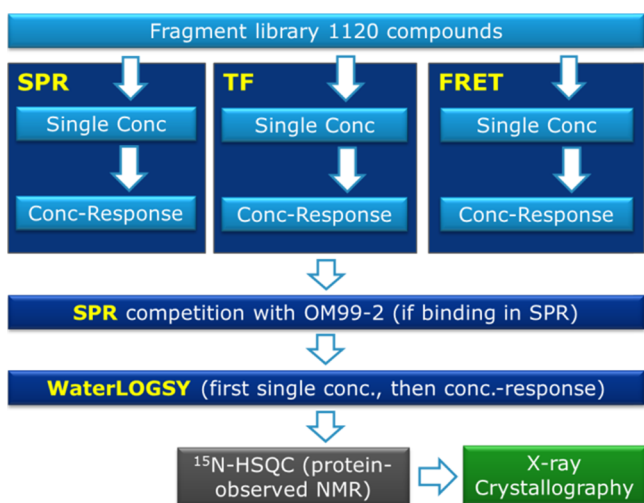


Figure 2. Hit identification and characterization flow chart used to identify non-Asp-binding fragments to BACE1.

D32N mutant allowed us to identify the catalytic Asp binding fragments. Fragment **10** was not tested because of its nonspecific binding behavior at pH 4.5 (very slow on/off rate constants).

Hit Analysis. The outcome from the three orthogonal primary assays, SPR, TF, and enzymatic FRET, is presented in Figure 3 and the corresponding data in Table 1. The criteria for

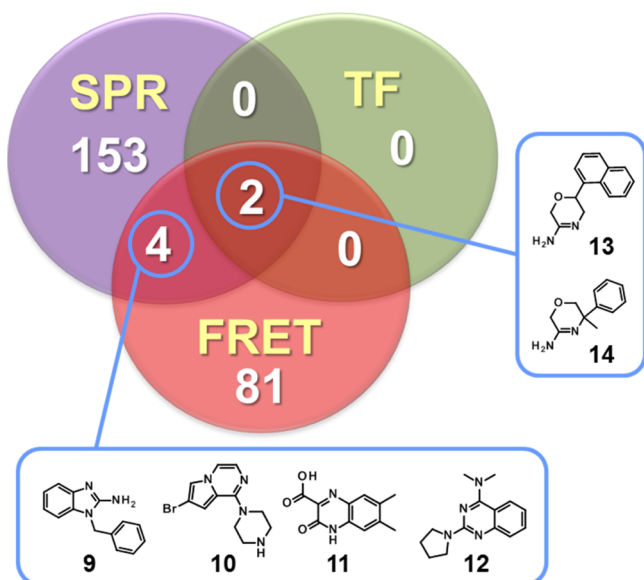


Figure 3. Hits identified across different fragment screens.

hit selection were as follows: SPR hits showed a specific and concentration-dependent binding at one or both pHs; TF hits gave a ΔT_m shift >0.5 °C at the highest concentration with no sign of autofluorescence; and FRET hits showed a robust CR curve and no autofluorescence. Of the three approaches, FRET gave 87 hits in total (7.8%), but a majority (81, 92%) did not confirm in other assays. Because of its high sensitivity, SPR gave the highest hit rate (159 hits: 77 at pH 7.4 and 106 at pH 4.5, with an overlap of 24 hits), with only 6 confirmed in other assays. Finally, TF gave the lowest amount of hits (2, 0.18%), but both confirmed in SPR and FRET. The structures of hits confirmed in at least two assays are shown in Figure 3.

Four compounds (**9–12**) showed SPR and enzymatic activity but no thermal shift (Figure 3 and Table 1). Of these, **9** bound to both WT and mutant BACE1 but also showed reduced binding in the presence of OM99-2, suggesting interaction with the catalytic Asp's. Fragment **9** contains a known guanidine motif⁴² and hence did not fit our criteria of novelty. Why **9** binds to the BACE1 D32N mutant despite its guanidine substructure remains elusive, but it may be indicative of nonspecific binding despite our efforts to filter out such false positives. The other fragments with overlapping SPR and FRET activity, **10–12**, were not previously reported to bind to BACE1. Fragment **10** bound to the BACE1 D32N mutant alone and in the presence of OM99-2, suggesting binding outside the catalytic site. Interestingly, fragments **11** and **12** do not display any known Asp-binding motif, bound to the BACE1 D32N mutant, and showed reduced binding in the presence of OM99-2. This strongly suggested that they bind to the active site without interaction with the catalytic Asps. The sensorgrams of **12** show binding in the absence (red) and presence (green) of OM99-2 and to the BACE1 D32N mutant (Figure 4). Finally, only two hits were confirmed in all three assays: **13** and **14**. However, **14** is an intermediate from a BACE1 medicinal chemistry exploration,²³ whereas **13** is a structurally related but much weaker binding compound synthesized for an unrelated project. For fragments **13** and **14**, K_D 's of respectively 0.83 and 0.12 mM could be calculated from the TF CR data. In SPR, **14** bound strongly to the mature BACE1 ectodomain but, in contrast to **13**, lost binding to the BACE1 D32N mutant (Figure 4C). Binding of **14** was also drastically reduced in the presence of OM99-2 (Figure 4A).

WaterLOGSY. In the preparation of eventual heteronuclear single-quantum coherence spectroscopy (HSQC) experiments, the binding of selected hits (**9–12** and **14**) was confirmed using WaterLOGSY, a ligand-observed NMR binding assessment technique (Table 1). A 30-fold excess of ligand was used at physiological pH. Experiments were repeated at pH 4.5.⁴³ Fragment **9** showed a very intense positive peak at pH 7.5, and also clear positive signals were observed for **10** and **12**. Signals for **11** and **14** were negative under these conditions. Nevertheless, when the experiments were repeated at acidic pH, a strong positive signal was obtained for **14**, whereas **11** remained negative.

Protein-Observed NMR. The partial assignment of amino acids in the mature BACE1 ectodomain via ¹⁵N-HSQC has been reported.⁴⁴ This technique was used to further characterize the binding of fragments **10** and **12** to BACE1 and as a selection criterion for X-ray crystallography. Being a known Asp binder, **14** was selected as a reference. Compound **9** and **13** were discarded given their similarity to previously reported hits, and **11** was excluded on the basis of WaterLOGSY experiments. BACE1 was labeled with ¹⁵N as necessary for the ¹⁵N-HSQC 2D experiment. The TROSY approach was employed as it produced better resolution, which is beneficial given the signal broadening and overlap in the spectra typically seen for large proteins. Most of the reported assignment could be annotated at the corresponding NH signals. A 5-fold excess of ligand was added to a 0.1 mM protein sample. To visualize shift changes upon interaction between the ligand and protein, the combined shift difference was calculated from the chemical shift differences in the nitrogen and the proton dimension, using the following formula.

Table 1. FRET, SPR, TF, and WL Data for Compounds 9–14^{a,b}

compd	FRET		SPR			TF			WaterLOGSY	
	IC ₅₀ (mM)	binding at pH 7.5	binding at pH 4.5	OM99-2 competition	D32N binding	Δ <i>T</i> _m (°C)	conc (mM)	<i>K</i> _D (mM)	signal at pH 7.5	signal at pH 4.5
9	1.6	yes	yes	minor	yes	−1.12	2.1		intense positive	NT
10	0.6	yes	SB ^d	no	yes	−0.27	2.1		positive	NT
11	0.4	yes	yes	minor	yes	0.15	0.8		negative	negative
12	0.5	yes	yes	minor	yes	NM ^c	2.1		positive	NT
13	1.1	yes	yes	minor	yes	0.63	2.1	0.83	NT	NT
14	0.2	yes	yes	yes	no	2.78	2.1	0.12	negative	intense positive

^aAverage of at least two independent runs, except WaterLOGSY, which was performed once. ^bNT, not tested. ^cNM, not measurable due to (auto)fluorescence interference. ^dSB, superstoichiometric binder.

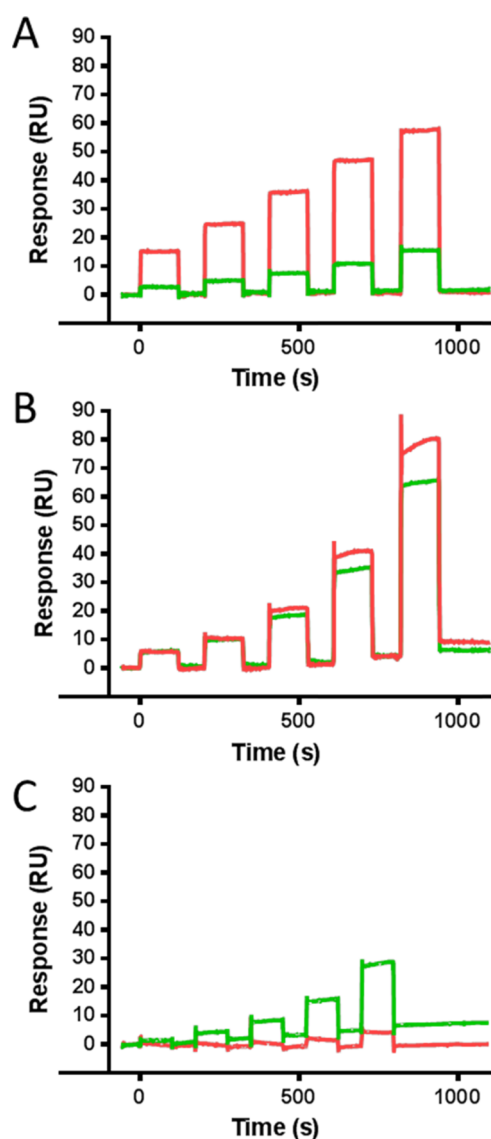


Figure 4. SPR sensorgrams showing the interaction of 14 (A) and 12 (B) to WT BACE1 before (red curve) and after (green curve) OM99-2 injection. (C) Sensorgrams of the binding of 12 (green curve) and 14 (red curve) to the BACE1 D32N mutant. The compounds were tested in CR series (0.03, 0.06, 0.13, 0.25, 0.50 mM).

combined shift difference

$$= [({}^1\text{H shifts})^2 + ({}^{15}\text{N shifts}/6.51)^2]^{0.5}$$

The 2D-HSQC results of 12 and 14 are shown in Figure 5. Amino acids from mature ¹⁵N-labeled BACE1 that experience changes upon interaction are displayed on the X axis, and the combined shift difference in parts per million (ppm) is represented on the Y axis. As expected, amino acids Asp32 and Asp228 were affected by the binding of 14, as well as neighboring amino acids Gly34 and Gly120. Interestingly, 12 affected different amino acids compared to 14. The shifts are visualized on the surface of the BACE1 protein extracted from the co-crystal with lead compound 4 (PDB 5CLM; Figure 6). Whereas 14 affected the two catalytic Asp's (shown in pink, adjacent to the amidine substructure, Figure 6A), 12 did not (Figure 6B). Instead, shifts were observed for multiple amino acids in the protein, with some close to the binding site such as Leu121, Arg128, Thr329, and Gly334. Unfortunately, a large number of amino acids in the active site were not assigned; therefore, the exact position of 12 could not be determined by NMR. In the case of 10, the observed chemical shift changes were much lower than those for compound 12 and no significant differences with 14 could be detected (data not shown).

Crystallography. Following the various primary assays and follow-up work, 12 emerged as the strongest candidate for attempting crystallography. Pleasingly, the screening, detailed analysis, and prioritization paid dividends as the crystal structure of 12 with BACE1 was readily solved at 2.5 Å resolution (PDB code 5MXD, Figure 7A). There are three copies of the BACE1–inhibitor complex in the crystallographic asymmetric unit, with each showing a similar binding mode of 12. The flexible active-site flap containing Tyr71 adopts different orientations in the three monomers.

In contrast to that in most known BACE1 inhibitors, such as 4, no interaction between 12 and the catalytic Asp dyad (Asp32 and Asp228) either directly or via a water-mediated network was seen (Figure 7C).²³ Instead, the quinazoline occupies the S1 pocket and the dimethylamine is oriented toward S3. Fragment 12 forms an H-bond between the protonated quinazoline and the backbone carbonyl of Phe108 in two of the three copies of BACE1 and forms π -stacking and hydrophobic interactions with residues Leu30, Tyr71, Phe108, Ile110, Trp115, and Ile118 (Figure 7B). The pyrrolidine ring goes into a new, more-solvent-exposed subpocket. The distance between the nitrogen of the dimethylamine and the carbonyl of Gly230 is too long to form a strong hydrogen bond (3.4–3.9 Å in the three copies).

Figure 7D compares the structures of reported non-Asp binders 6 and 8 to BACE1 with that of 12. Inhibitor 6 occupies a similar region but has some differences.²⁷ It also forms a H-

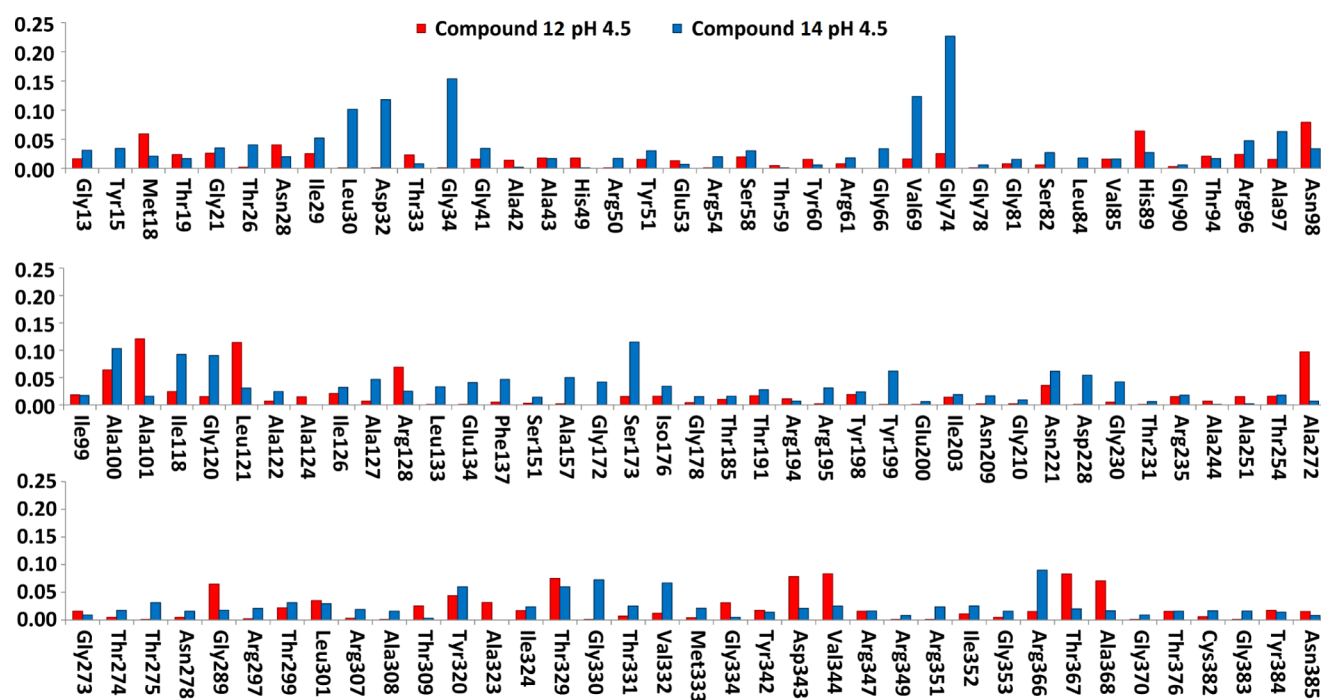


Figure 5. Chemical shift changes in BACE1 upon interaction with fragments 12 and 14. The three plots show the amino acids experiencing alterations in their 2D-HSQC ^{15}N shifts calculated according to the combined shift difference equation provided in the text.

bond with the carbonyl of Phe108; however, a sulfonamide is oriented toward S3 compared with the dimethylamine in 12. The dihydroisoquinolines 7 and 8 do not interact with Phe108 but, instead, form an H-bond network in S2, compensating for the absence of interaction with the catalytic Asp dyad.^{28,29}

CONCLUSIONS

Fragment screening with SPR, TF, and enzymatic FRET approaches delivered six hits, confirmed in at least two assays, and two in all three. The use of the BACE1 D32N mutant identified fragments that bind to BACE1 but not via Asp interactions. Further SPR competition experiments with OM99-2 helped in selecting those that bind to the catalytic cleft. After confirming binding by NMR (WaterLOGSY), protein-observed NMR using ^{15}N -labeled BACE1 led to the prioritization of 12 for X-ray crystallography, which revealed a unique binding mode in the S2 pocket of BACE1. This orthogonal screening cascade along with mutant and competition experiments is a valid general approach for finding novel ligands for drug discovery targets, especially when the IP space is dominated by similar chemical motifs. In addition, this orthogonal screening paradigm maximizes the chance to obtain X-ray structures of such ligands with unusual binding modes.

METHODS

Proteins. The mature BACE1 ectodomain protein (amino acid residues -16 to 393) with a COOH-terminal 6xHis-tag (denoted “mature BACE1 ectodomain” throughout the article) was expressed by baculovirus infection of HighFive insect cells and purified from the cell culture supernatant using Ni-NTA affinity chromatography, anion exchange chromatography, and size-exclusion chromatography essentially as described by Bruinzeel et al.⁴⁵ The mature BACE1 ectodomain catalytic-site mutant (D32N) protein (amino acid residues -16 to 393) with a COOH-terminal 6xHis-tag and StrepII-tag was expressed

in and purified from *E. coli* cells by the Protein Service Facility of the University of Ghent.⁴⁶ The only difference between the WT and mutant forms of the protein (apart from the mutation) is the somewhat longer tag at the COOH-terminus of the mutant form (only 9 amino acid residues for His-tag vs 21 amino acid residues for His- + Strep-tag). The BACE1 ectodomain has been tagged at the COOH-terminus in many studies, and no apparent effect on its activity or conformation has been described. Although an experimental effect of the tag and/or the difference in length between the tags cannot be excluded, it is highly unlikely. For ^{15}N -HSQC NMR experiments, labeled BACE1 (amino acid residues -16 to 393) was expressed in minimal medium with $^{15}\text{NH}_4\text{Cl}$ from *E. coli* cells and purified by ion-exchange and size-exclusion chromatography by the Structural Biochemistry Laboratory of the CIPF.⁴⁷

FRET. Primary BACE1 enzymatic activity was assessed by a FRET assay using an APP-derived 13 amino acids peptide, that contains the “Swedish” Lys-Met/Asn-Leu mutation of the APP β -secretase cleavage site, as a substrate (MCA -Ser-Glu-Val-Asn-Leu-Asp-Ala-Glu-Phe-Arg-Lys(DNP)-Arg-Arg-NH₂ TFA salt, Bachem cat No. M-2465) and a mature BACE1 ectodomain (Aurigene, custom-made). The substrate contains fluorophore MCA as a fluorescent donor with excitation wavelength at 320 nm and emission wavelength at 405 nm and proprietary quencher acceptor DNP. The distance between these two groups has been selected so that upon light excitation the donor fluorescence energy is significantly quenched by the acceptor, through resonance energy transfer. Upon cleavage by BACE1, MCA is separated from DNP, restoring the full fluorescence yield of the donor. The increase in fluorescence is linearly related to the rate of proteolysis. In a 384-well format, BACE1 is incubated for 2 h with the substrate and the inhibitor. The amount of proteolysis is directly measured by fluorescence measurement in the Fluoroskan microplate fluorometer (Thermo Scientific). For the low control, no enzyme was added to the reaction mixture. The enzymatic BACE1 FRET

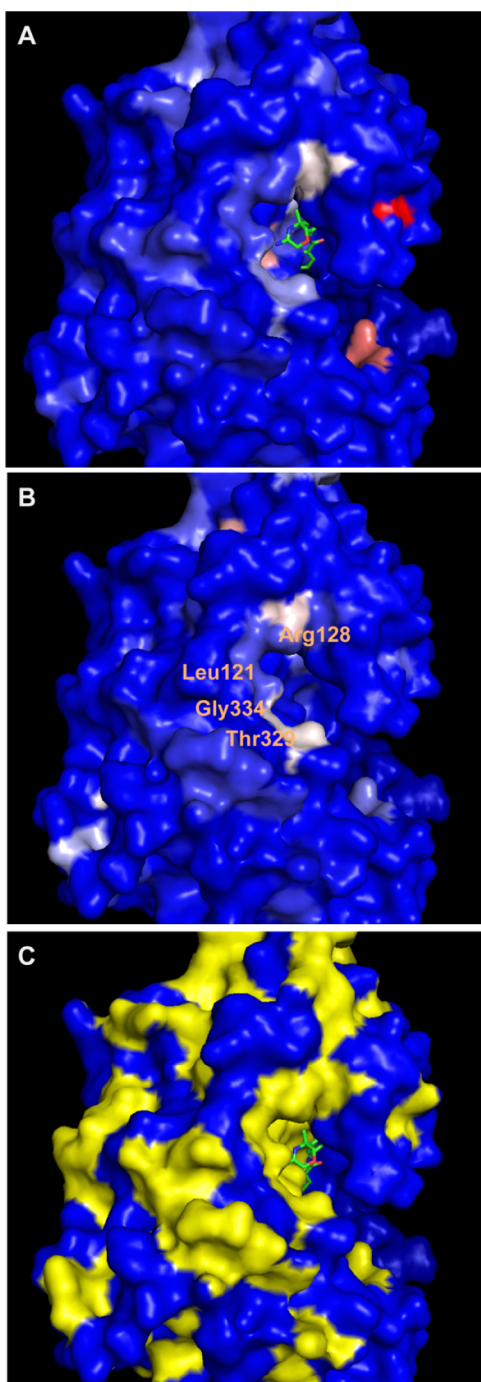


Figure 6. Visualization of ^{15}N -HSQC shift changes with **14** (A) and **12** (B) using the co-structure of **4** with BACE1 (PDB 5CLM): blue, no change; light blue, 0–0.04 ppm; white, 0.05–0.08 ppm; pink, 0.05–0.11 ppm; and red, 0.11–0.15 ppm. (C) The assigned amino acids are shown in yellow. The structure of **4** is shown in green in (A) and (C).

assay was performed in a total volume of 30 μL in a buffer containing 33.3 mM citrate, pH 5.0; 0.033% PEG; 10 μM substrate; 32.4 nM BACE1; and the compound. Compound stock solutions in 100% DMSO were diluted, 1/33.3, in the reaction mixture, resulting in final DMSO concentrations of 4% (3% from compound, 1% from substrate).

SPR. Measurements were performed using a Biacore 4000 instrument and CM7 biosensor chips (GE Healthcare). The mature BACE1 ectodomain and neutravidin both were

immobilized by amine coupling using standard procedures and materials provided by GE Healthcare. A mixture of Hepes (10 mM), pH 7.4, NaCl (150 mM; HBS-N), and 0.005% Tween 20 was used as the running buffer during immobilization. Interaction experiments were performed at 25 $^{\circ}\text{C}$ at both pH 7.4 (running buffer HBS-N, pH 7.4, with 0.05% Tween 20 and 5% DMSO) and pH 4.5 (running buffer 10 mM NaOAc, pH 4.5, with 150 mM NaCl, 0.05% Tween 20, and 5% DMSO). Fragments and reference compounds were injected for 30 s over the sensor surface at a flow rate of 30 $\mu\text{L}/\text{min}$. DMSO solvent correction was performed using calibration points containing between 2.5 and 6.5% DMSO. Binding response of reference compounds was followed during the fragment screen to determine potential decrease in the apparent analyte binding capacity of BACE1, which was compensated for in the data analysis. Data analysis has been performed using the Biacore 4000 Control and Evaluation software and Excel. Fragments were screened twice (forward and reverse order) at 0.25 mM and at pH 7.4 and 4.5 against BACE1, neutravidin, and a blank reference spot to identify and discard promiscuous binders. For the primary screen, fragments have been tested at 0.25 mM in duplicate both at pH 7.4 and 4.5. Top 10% screening hits were retested by CR curves, ranging between 0.03 and 0.500 mM (8 concentrations with 1.5-fold dilution range). Competition experiments (pH 4.5) were performed by injection of fragment hits before and after injection of the OM99-2 peptide (Calbiochem, 496000). Immobilization and SPR measurements using the BACE1 D32N mutant were performed under the conditions similar to those used for WT BACE1.

ThermoFluor. The BACE1 ThermoFluor assay was performed in 384-well plates in a total volume of 4 μL in a buffer containing 50 mM NaOAc pH 5.4, 150 mM NaCl, 0.0005% Tween 20, 100 μM ANS, 1.6 μM mature BACE1 ectodomain protein and compound. Compound stock solutions in 100% DMSO were diluted 1/24 in the reaction, resulting in final compound concentrations of 2.1, 0.80, or 0.2 mM (depending on the initial compound stock concentration) and a final DMSO concentration of 4.2%. Thermal shift measurements were done in a ThermoFluor instrument from 25 to 85 $^{\circ}\text{C}$ in 1 $^{\circ}\text{C}$ increments. Fluorescence at every temperature was determined using a charge-coupled device camera and subsequent image analysis using proprietary software.

WaterLOGSY and Protein-Observed NMR. All NMR experiments were performed using a Bruker Avance II 600 MHz spectrometer equipped with a 5 mm inverse cryoprobe at 27 $^{\circ}\text{C}$. For WaterLOGSY experiments, to 480 μL of 5 μM mature BACE1 ectodomain, 20 μL of D_2O and 0.15 mM of ligand were added (from a 100 mM stock in $\text{DMSO}-d_6$), in a protein/ligand ratio of 1:30, optimal for the WaterLOGSY experiments. For each sample, 1D ^1H and WaterLOGSY experiments were conducted. A total of 32 K -points were used for a sweep width of 14 ppm, and a total of 128 scans were accumulated for the WaterLOGSY experiment. For ^{15}N -HSQC NMR experiments, protein samples were concentrated to 0.10 mM, and 0.02 mL of D_2O and 0.50 mM of ligand were added (from a 100 mM stock in $\text{DMSO}-d_6$) to 0.48 mL of protein sample. The TROSY version of ^{15}N -HSQC with sensitivity enhancement was acquired with 200 scans, spectral widths of 14 and 40 ppm and offsets of 4.7 and 117 ppm in the ^1H and the ^{15}N dimension, respectively. Spectra were acquired and processed with Topspin 3.2 (Bruker Biospin), and 2D experiments were integrated with Sparky (T. D. Goddard and

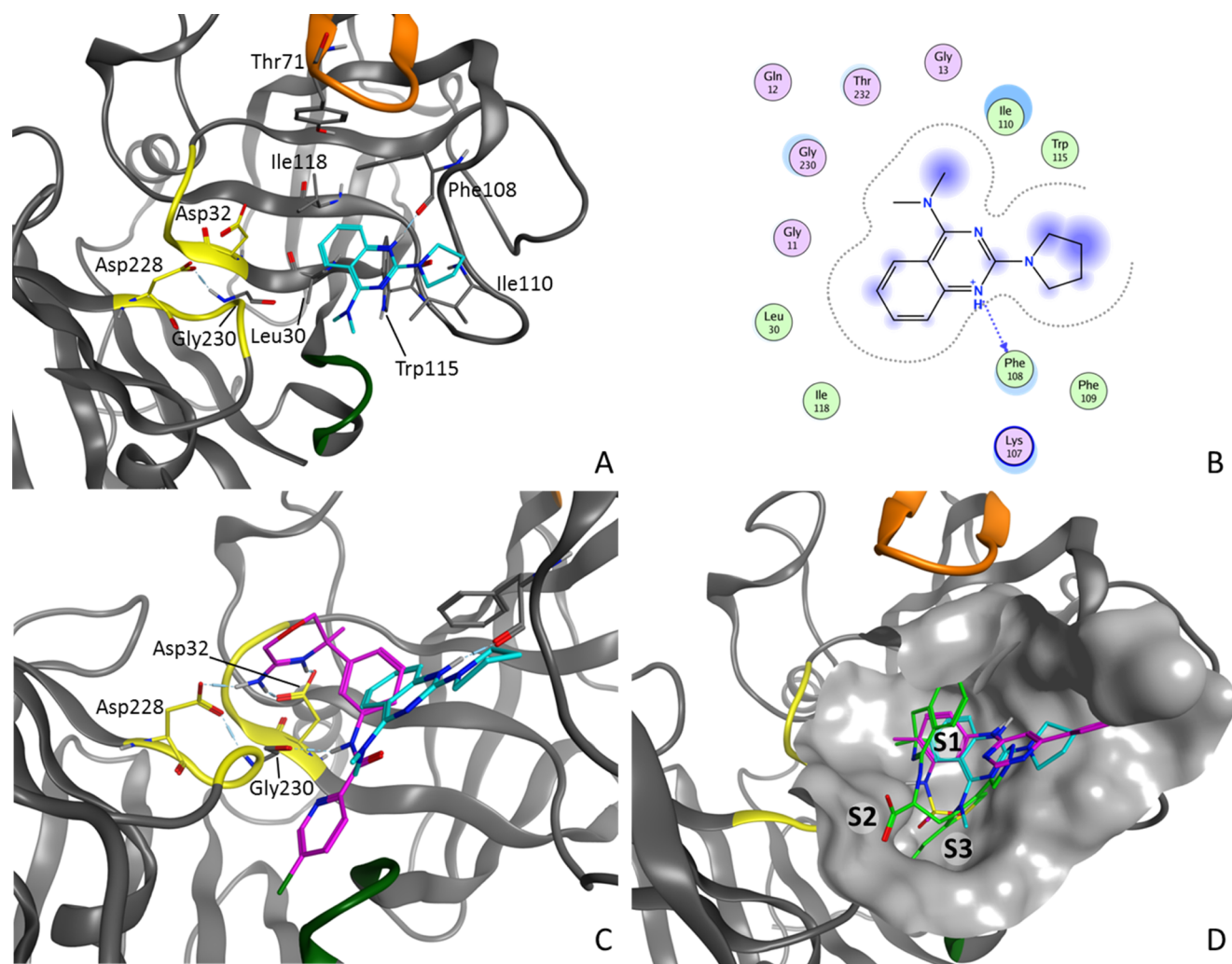


Figure 7. Interactions of 12 (A), interaction map of 12 (B), a comparison between the binding modes of 12 and Asp binder 4 (C), and a comparison of the binding modes of non-Asp binders 6 (magenta), 8 (green), and 12 (cyan) (D).

D. G. Kneller; SPARKY 3, University of California, San Francisco).

Crystal Structure Experimental Data. A structure of 12 in BACE1 (1–454) was obtained by Proteros Biostructures GmbH.⁴⁸ X-ray crystallography data collection and refinement statistics are summarized in Table 2, and refinement statistics are summarized in Table 3. Human BACE-1 (amino acids 22–446 preceded by MetHis6; numbering as in UniProtKB entry P56817) was expressed in *E. coli* BL21(DE3) in inclusion bodies. Briefly, inclusion bodies were refolded from 8 M urea and further purified by ion-exchange and gel-filtration chromatography. After the removal of the propeptide by digestion with clostripain, the noncleaved material was removed by NiNTA chromatography and the protein was finally subjected to ion-exchange chromatography. For crystallization, the protein was concentrated to 23 mg/mL, flash-frozen in liquid nitrogen, and stored at $-80\text{ }^{\circ}\text{C}$ until further use.

For crystallization, the protein at 10 mg/mL was incubated for 1 h on ice with 2 mM of the ligand (diluted from 100 mM DMSO stock in the protein solution). The protein was crystallized from 12% (m/v) PEG4000, 100 mM MES/NaOH, pH 5.5, by hanging-drop vapor diffusion at $20\text{ }^{\circ}\text{C}$ ($0.75\text{ }\mu\text{L}$ protein + $0.75\text{ }\mu\text{L}$ reservoir solution). For cryoprotection,

Table 2. Data Collection and Processing Statistics for 12

ligand	12
PDB ID	5MXD
X-ray source	PXI/X06SA (SLS) ^a
wavelength [Å]	0.99999
detector	PILATUS 6M
temperature [K]	100
space group	C2
cell: <i>a</i> ; <i>b</i> ; <i>c</i> ; [Å]	232.91; 100.74; 59.05
cell: α ; β ; γ ; [deg]	90.0; 102.0; 90.0
resolution [Å]	2.52 (2.77 – 2.52) ^b
unique reflections	43 635 (10 835) ^b
multiplicity	2.9 (2.9) ^b
completeness [%]	96.5 (97.5) ^b
R_{sym} [%]	6.6 (50.6) ^b
R_{meas} [%]	8.1 (61.7) ^b
mean(<i>I</i>)/sd	13.64 (2.44) ^b

^aSwiss Light Source (SLS, Villigen, Switzerland). ^bValues in parentheses refer to the resolution bin with $R_{\text{sym}} = 50.6\%$.

crystals were briefly soaked in reservoir solution mixed with 25% (v/v) glycerol and frozen in liquid nitrogen.

Table 3. Refinement Statistics

resolution [Å]	113.90–2.52
number of reflections (working/test)	42 644/991
R_{cryst} [%]	22.7
R_{free} [%]	28.1
total number of atoms	
protein	8960
water	
ligand	54
deviation from ideal geometry	
bond lengths [Å]	0.007
bond angles [deg]	1.23
bonded B's [Å ²]	3.5
Ramachandran plot	
most favored regions [%]	87.5
additional allowed regions [%]	11.9
generously allowed regions [%]	0.3
disallowed regions [%]	0.3

X-ray diffraction data were collected at the SLS (beamline PXI/X06SA) using a PILATUS 6M detector. Data were integrated, scaled, and merged using XDS.⁴⁹ The structure was refined with REFMACS.⁵⁰ Manual model completion was carried out using Coot.⁵¹ The quality of the final model was verified by PROCHECK⁵² and the validation tools available through Coot.⁵¹

Chemistry. Compound **9** was obtained commercially from Specs and Biospecs (CAS# 43182-10-1) and has been described before.⁵³ Compound **11** was obtained from the internal compound collection and has been previously reported.⁵⁴

Analytical Methods. All final compounds were characterized by ¹H NMR and LC/MS and were >95% pure by ¹H NMR. ¹H NMR spectra were recorded on Bruker spectrometers: DPX-360 MHz, AVI-500 MHz, and AVI-600 MHz. For ¹H NMR spectra, all chemical shifts are reported in ppm (δ) units and are relative to the residual signal at 7.26 and 2.50 ppm for CHCl₃ and DMSO, respectively. Different LC/MS methods were used to characterize the products. LC/MS method A. Instrument: Waters Alliance HT 2790 - DAD-MS; column: Xterra MS C18 (3.5 μ m, 4.6 \times 100 mm²); eluent: (A) 95% NH₄OAc 25 mM + 5% ACN, (B) ACN, (C) MeOH; gradient from 100% A to 50% B and 50% C in 6.5 min, to 100% B in 1 min, 100% B for 1 min and re-equilibrate with 100% A for 1.5 min; flow 1.6 mL/min; column T: 40 °C; run time: 10 min. LC/MS Method B. Instrument: Waters Acquity UPLC - DAD and SQD; column: waters: BEH C18 (1.7 μ m, 2.1 \times 50 mm²); eluent: (A) 95% NH₄OAc 6.5 mM + 5% ACN, (B) ACN; gradient from 95% A to 40% A in 3.8 min to 5% A in 0.8 min held for 0.4 min; flow: 1 mL/min; column T: 50 °C; run time: 5 min. LC/MS Method C. Instrument Waters Acquity UPLC - DAD and SQD; column: BEH C18 (1.7 μ m, 2.1 \times 50 mm²; Waters Acquity); eluent: (A) 95% NH₄OAc 25 mM + 5% ACN, (B) ACN; gradient from 95% A and 5% B to 5% A and 95% B in 1.3 min and hold for 0.3 min; flow: 0.8 mL/min; column T: 55 °C; run time: 2 min. LC/MS Method D. Instrument Waters Acquity UPLC - DAD and SQD; column: Waters HSS T3 (1.8 μ m, 2.1 \times 100 mm²); eluent A: 10 mM NH₄OAc in 95% H₂O + 5% ACN, (B) ACN; gradient from 100% A to 5% A in 2.10 min, to 0% A in 0.90 min, to 5% A in 0.5 min; flow: 0.7 mL/min; column T: 55 °C; run time 3.5 min.

Experimental Procedures. Scheme 1 outlines the routes used to prepare compounds **10**, **12**–**14**.

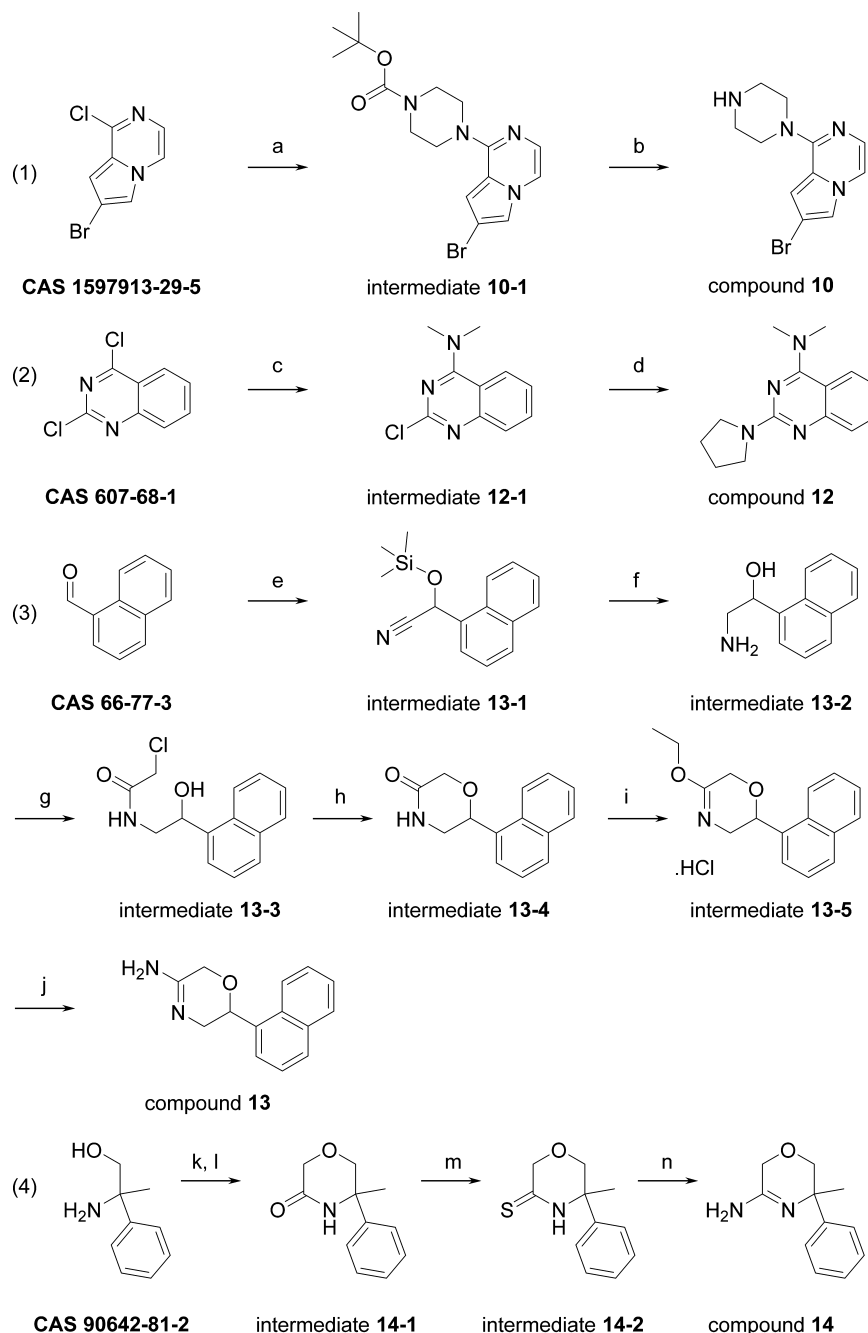
7-Bromo-1-piperazin-1-yl-pyrrolo[1,2-*a*]pyrazine (**10**). 7-Bromo-1-chloro-pyrrolo[1,2-*a*]pyrazine (0.4 g, 1.7 mmol, CAS 1597913-29-5), 1-Boc-piperazine (0.633 g, 3.4 mmol, CAS 143238-38-4) and K₂CO₃ (0.47 g, 3.4 mmol) in ACN (7.5 mL) were heated in a microwave oven for 15 min at 170 °C. Then, additional 1-Boc-piperazine (0.633 g, 3.4 mmol, CAS 143238-38-4) was added and the reaction was heated at 180 °C for 45 min. After cooling to rt, DCM was added, the solid was filtered off, and the filtrate solvent was evaporated affording 1.0 g of intermediate **10-1** (100%).

Intermediate **10-1** (1.0 g, 1.7 mmol) in 6 N HCl/2-propanol (10 mL) was stirred for 1 h at room temperature (rt). Then, DCM and aqueous saturated Na₂CO₃ were added. The organic layer was separated, dried (Na₂SO₄), filtered, and the solvent was evaporated. The residue was purified by column chromatography (eluent: DCM/(7 N NH₃ in MeOH), 96:4), affording 430 mg of compound **10** (90%). ¹H NMR (600 MHz, DMSO-*d*₆): δ ppm 2.78–2.85 (m, 4H), 3.47–3.50 (m, 4H), 6.84 (dd, *J* = 1.5, 0.9 Hz, 1H), 7.12 (d, *J* = 4.6 Hz, 1H), 7.70 (dd, *J* = 4.7, 0.9 Hz, 1H), 7.74 (d, *J* = 1.5 Hz, 1H); LC/MS (method D); *R*_t 1.22 min, MH⁺ 281.

N,N-Dimethyl-2-pyrrolidin-1-yl-quinazolin-4-amine (**12**). Dimethylamine (2 M solution in THF, 22.6 mL, 45.22 mmol, CAS 607-68-1) was added dropwise to a slurry of 2,4-dichloroquinazoline (3000 mg, 15.07 mmol) in THF (10 mL)/water (15 mL). The resulting mixture was stirred for 17 h at rt and then poured into water and extracted with EtOAc (3 \times 75 mL). The combined extracts were dried (MgSO₄), filtered, and concentrated in vacuo, yielding intermediate **12-1** as a bright white powder (3.16 g, 100%). LC/MS (method C); *rt* 0.84 min, MH⁺ 208.

A MW-vessel was charged with intermediate **12-1** (0.25 g, 1.20 mmol), pyrrolidine (301 μ L, 3.61 mmol), and ACN (5 mL). This mixture was stirred and heated under MW irradiation at 110 °C for 30 min. Next, the reaction mixture was concentrated in vacuo and purified using RP-HPLC (RP Shandon Hyperprep C18 BDS – 10 μ m, 250 g, 5 cm, mobile phase (0.25% NH₄HCO₃ solution in water, MeOH + ACN)). The desired fractions were concentrated in vacuo and co-evaporated twice with MeOH at 60 °C. An off-white solid was obtained, which was dissolved in 10 mL of DCM. This solution was then treated with NaOH (1 mL, 1 M), dried over an Isolute HM-N tube, and rinsed with 10 mL of DCM. The collected solution was evaporated at 50 °C under a stream of nitrogen. The residue was dissolved in 15 mL of DCM, and 1.5 equiv of HCl (6 N in 2-propanol) was added dropwise. The obtained solution was then stirred for 1 h. The white crystals were collected on a filter, rinsed with 10 mL of DCM, and dried in a vacuum oven at 55 °C for 24 h, yielding compound **12** (242 mg, 83%) as a white powder. ¹H NMR (600 MHz, DMSO-*d*₆): δ ppm 1.95 (br. s, 2H), 2.04 (br. s, 2H), 3.47 (br. s, 6H), 3.67 (t, *J* = 6.8 Hz, 4H), 7.37 (t, *J* = 7.7 Hz, 1H), 7.78 (t, *J* = 7.7 Hz, 1H), 7.94 (d, *J* = 8.3 Hz, 1H), 8.17 (d, *J* = 8.3 Hz, 1H), 12.05 (s, 1H); LC/MS (method A); *R*_t 4.24 min, MH⁺ 243.

2-(1-Naphthyl)-3,6-dihydro-2*H*-1,4-oxazin-5-amine (**13**). Zinc(II) iodide (0.025 g, 0.078 mmol) was added to 1-naphthaldehyde (36.4 g, 0.233 mol, CAS 66-77-3), and the resulting mixture was cooled with ice. Next, TMSCN (25 g, 0.252 mol) was added dropwise. When the addition was complete, the mixture was brought to 25 °C. After the reaction

Scheme 1. Synthesis of Compounds 10, 12–14^a

^aReagents and conditions: (a) 1-Boc-piperazine, K_2CO_3 , ACN, rt, 1 h. (b) 6 N HCl/2-propanol, rt, 1 h. (c) $NHMe_2$ (2 M in THF), THF/water, 17 h, rt. (d) pyrrolidine, ACN, microwave 110 °C, 3 h. (e) TMS-CN, ZnI_2 , 0 °C to rt, 2 days. (f) $LiAlH_4$, Et_2O , rt, 2 days. (g) $ClCH_2COCl$, NEt_3 , DCM, 0 °C to rt, 30 min. (h) NaH, 2-propanol, rt, overnight. (i) Epichlorohydrin, BF_3OEt_2 , Et_2O , rt, overnight. (j) 7 N NH_3 /MeOH, rt, overnight. (k) $ClCH_2COCl$, DIPEA, THF, -10 to -5 °C. (l) t -BuOK, 5–10 °C, 60 min. (m) P_2S_5 , THF, 50 °C, 30 min. (n) NH_4OH , 40 °C, 11 h.

was judged complete (thin-layer chromatography (TLC) monitoring), the mixture was diluted with DCM and washed with an aqueous saturated $NaHCO_3$ solution. The organic layer was dried (Na_2SO_4), filtered, and concentrated to provide intermediate 13-1 as a red-orange oil that solidified upon standing (59.97 g, 100%).

In a three-necked flask fitted with a mechanical stirrer and addition funnel, $LiAlH_4$ (9.90 g, 0.261 mol) was suspended in dry diethyl ether (205 mL) under nitrogen flow. Next, intermediate 13-1 (59.50 g, 0.233 mol) dissolved in 75 mL dry diethyl ether was added dropwise. When the addition was

complete, the reaction was stirred at rt until judged complete by TLC monitoring (about 2 days). Next, 10 mL water was added dropwise, followed by 10 mL of a 15% NaOH solution. Then, 29.7 mL of water was again added carefully. The mixture was further stirred until a precipitate was formed, which was filtered over dicalite. The filtrate was concentrated, providing intermediate 13-2 as a bright orange-red oil (13.9 g, 32%).

Intermediate 13-2 (13.8 g, 0.737 mol) was dissolved in 500 mL dry DCM. Triethylamine (14.9 g, 0.147 mol) was added, and the resulting solution was cooled with ice. Next, chloroacetyl chloride (9.99 g, 0.0884 mol) was added dropwise,

and after addition, the reaction mixture was allowed to warm to rt. After the reaction was judged complete (TLC monitoring), the mixture was poured into 1 N HCl (500 mL). The organic layer was separated, and the aqueous layer was extracted with DCM (3 × 250 mL). The combined organic layers were dried (Na₂SO₄), filtered, and evaporated to dryness. The residue was purified over silica gel using CHCl₃ as eluent. The product fractions were evaporated, yielding intermediate 13-3 as a beige foam (6.10 g, 31%).

Sodium hydride (60% dispersion in mineral oil, 1.85 g, 0.463 mmol) was washed with dry hexanes, and then, 76 mL of dry 2-propanol was added. The resulting mixture was stirred for 2.5 h at 25 °C. Next, intermediate 13-3 (6.10 g, 0.0232 mol) in 78 mL of 2-propanol was added. The reaction mixture was stirred overnight at 25 °C. Then, the reaction was quenched by pouring the mixture into 110 mL of ice-water containing HOAc (1.30 mL, 0.0232 mol). The mixture was extracted with CHCl₃ (2 × 250 mL). The combined organic layers were dried (Na₂SO₄), filtered, and evaporated to dryness. The residue was purified over silica gel using CHCl₃/MeOH (99:1) as eluent, yielding intermediate 13-4 (2.88 g, 55%).

Boron trifluoride diethyl etherate (1.34 g, 0.00944 mol) was dissolved in 5.6 mL of dry diethyl ether. Epichlorohydrin (0.68 g, 0.00726 mol) was added, and the resulting mixture was stirred for 2 h at 25 °C. Next, the ether was decanted and the residue was washed with ether. DCM (11 mL) was added to the residue, and intermediate 13-4 (1.65 g, 0.00726 mol) in 11 mL DCM was subsequently added. The resulting mixture was stirred overnight at 25 °C, after which all volatiles were evaporated, providing intermediate 13-5 as a light yellow foam, which was carried as such to the next reaction step.

Intermediate 13-5 (crude from previous step, approx. 0.00726 mol) was dissolved in 15.6 mL of NH₃ in MeOH (7 N, 0.109 mol), and the resulting mixture was stirred overnight at rt. Next, 1 N NaOH (50 mL) was added, and the mixture was extracted with CHCl₃ (3 × 50 mL). The combined organic layers were dried (Na₂SO₄), filtered, and evaporated. Diethyl ether was added to the residue, followed by concentrated HCl (0.61 mL, 0.00726 mol). The resulting precipitate was filtered, and recrystallized from MeOH/Et₂O, yielding compound 13 as a white solid (0.66 g, 46% two steps). ¹H NMR (600 MHz, DMSO-*d*₆): δ ppm 3.57 (dd, *J* = 13.2, 10.4 Hz, 1H), 3.75 (dd, *J* = 13.2, 3.3 Hz, 1H), 4.81 (d, *J* = 17.3 Hz, 1H), 4.87 (d, *J* = 17.3 Hz, 1H), 5.69 (dd, *J* = 10.4, 3.3 Hz, 1H), 7.53–7.65 (m, 4H), 7.92–8.01 (m, 2H), 8.19 (d, *J* = 8.4 Hz, 1H), 9.01 (br. s, 2H), 10.20 (br. s, 1H); LC/MS (method D); *R*_t 1.31 min, MH⁺ 227. Anal. Calcd for C₁₄H₁₄N₂O. HCl: C, 64.00; H, 5.75; N, 10.66; Cl, 13.49. Found: C, 63.01; H, 5.66; N, 10.17; Cl, 13.03. Mp 213–215 °C.

5-Methyl-5-phenyl-2,6-dihydro-1,4-oxazin-3-amine (14). To 2-amino-2-phenyl-propan-1-ol (1000 mg, 6.613 mmol, CAS 90642-81-2) and DIPEA (1.37 mL, 7.94 mmol) in THF (40 mL) at –10 °C was added chloroacetyl chloride (0.527 mL, 6.61 mmol) dropwise. Then, the mixture was left stirring while slowly warming up to –5 °C for 20 min. Then, *t*-BuOK (1.86 g, 16.53 mmol) was added portionwise, and the mixture was left warming up slowly to 5–10 °C for 60 min. Then, the reaction was quenched with 10% aq. NH₄Cl and extracted with DCM. The organic layers were dried (Na₂SO₄), filtered, evaporated, and purified by automated flash silica column (eluent: DCM/EtOAc, gradient 1:0 to 7:3), giving intermediate 14-1 as a transparent oil (870 mg, 69%). ¹H NMR (500 MHz, chloroform-*d*): δ ppm 1.70 (s, 3H), 3.74 (d, *J* = 11.6 Hz,

1H), 3.80 (d, *J* = 11.6 Hz, 1H), 4.21 (d, *J* = 16.8 Hz, 1H), 4.26 (d, *J* = 16.8 Hz, 1H), 6.41 (br. s, 1H), 7.29–7.36 (m, 1H), 7.37–7.44 (m, 4H); LC/MS (method D); *rt* 1.27 min, MH⁺ 192.

Intermediate 14-1 (400 mg, 2.092 mmol) and P₂S₅ (511 mg, 2.301 mmol) were dissolved in THF (15 mL), and the mixture was stirred at 50 °C for 30 min. Then, the mixture was cooled to rt and filtered over cotton and evaporated. The residue was dissolved in DCM and directly injected into a flash silica column, eluting with DCM. Evaporation of the product fractions provided intermediate 14-2 as a yellow oil (360 mg, 83%). ¹H NMR (500 MHz, chloroform-*d*): δ ppm 1.75 (s, 3H), 3.79 (d, *J* = 11.6 Hz, 1H), 3.84 (d, *J* = 11.6 Hz, 1H), 4.58 (d, *J* = 18.5 Hz, 1H), 4.65 (d, *J* = 18.5 Hz, 1H), 7.32–7.38 (m, 3H), 7.39–7.46 (m, 2H), 8.35 (br. s, 1H); LC/MS (method B); *R*_t 1.22 min, MH⁺ 208.

Intermediate 14-2 (340 mg, 1.64 mmol) was dissolved in NH₄OH (15 mL), and the mixture was stirred at rt overnight and then for 11 h at 40 °C. Then, water and DCM were added, the organic layer was separated, and the aqueous layer was further extracted with DCM (3×). The combined organic layers were dried (Na₂SO₄), filtered, and evaporated. Then, DCM (15 mL) and TFA (0.25 mL) were added, mixed well, and evaporated. Et₂O (20 mL) was added to the residue and sonicated. This formed a white precipitate, which was filtered and washed with Et₂O and dried. Then, this product was further purified by automated flash silica column (eluent (1% TFA in DCM)/MeOH; gradient 100:0 to 95:5). The fractions containing the product were collected and evaporated, and the residue was precipitated in Et₂O, filtered, and dried in vacuo. This gave intermediate 14 as a white solid (310 mg, 62%). ¹H NMR (500 MHz, DMSO-*d*₆): δ ppm 1.63 (s, 3H), 3.87 (d, *J* = 11.8 Hz, 1H), 3.93 (d, *J* = 12.1 Hz, 1H), 4.53–4.61 (m, 2H), 7.32–7.38 (m, 1H), 7.39–7.45 (m, 4H), 8.74 (br. s, 1H), 9.03 (br. s, 1H), 10.69 (s, 1H); LC/MS (method B); *R*_t 0.49 min, MH⁺ 191.

AUTHOR INFORMATION

Corresponding Author

*E-mail: frombout@its.jnj.com. Phone: +3214608216.

ORCID

Frederik J. R. Rombouts: 0000-0003-1986-0476

Andrés A. Trabanco: 0000-0002-4225-758X

Gary Tresadern: 0000-0002-4801-1644

Present Address

[†]This author is presently also affiliated with the Instituto de Investigación Sanitaria La Fe, Drug Discovery Unit, Avda. Fernando Abril Martorell 106, 46026 Valencia, Spain (A.P.-L.).

Author Contributions

The manuscript was written through contributions of all authors. All authors have given approval to the final version of the manuscript.

Notes

The authors declare no competing financial interest.

ACKNOWLEDGMENTS

We thank Proteros for BACE1 crystal growth, soaking, and structure determination of 12.⁴⁸

■ ABBREVIATIONS

BACE1, β -secretase 1; DNP, 2,4-dinitrophenyl; FRET, fluorescence resonance energy transfer; HTS, high-throughput screening; MCA, (7-methoxycoumarin-4-yl) acetic acid; DNP, 2,4-dinitrophenyl; SPR, surface plasmon resonance; TF, ThermoFluor; TROSY, transverse relaxation optimized spectroscopy; JFL, Janssen Fragment Library; CR, concentration-response

■ REFERENCES

- (1) Hebert, L. E.; Weuve, J.; Scherr, P. A.; Evans, D. A. Alzheimer disease in the United States (2010–2050) estimated using the 2010 census. *Neurology* **2013**, *80*, 1778–1783.
- (2) Dementia; Fact Sheet April, 2016. World Health Organization Website. <http://www.who.int/mediacentre/factsheets/fs362/en/> (accessed Nov 8, 2016).
- (3) Yiannopoulou, K. G.; Papageorgiou, S. G. Current and future treatments for Alzheimer's disease. *Ther. Adv. Neurol. Disord.* **2013**, *6*, 19–33.
- (4) Hüll, M.; Berger, M.; Heneka, M. Disease-modifying therapies in Alzheimer's disease: how far have we come? *Drugs* **2006**, *66*, 2075–2093.
- (5) Citron, M. Alzheimer's disease: strategies for disease modification. *Nat. Rev. Drug Discovery* **2010**, *9*, 387–398.
- (6) Leger, G. C.; Massoud, F. Novel disease-modifying therapeutics for the treatment of Alzheimer's disease. *Exp. Rev. Clin. Pharmacol.* **2013**, *6*, 423–442.
- (7) Hussain, I.; Powell, D.; Howlett, D. R.; Tew, D. G.; Meek, T. D.; Chapman, C.; Gloger, I. S.; Murphy, K. E.; Southan, C. D.; Ryan, D. M.; Smith, T. S.; Simmons, D. L.; Walsh, F. S.; Dingwall, C.; Christie, G. Identification of a novel aspartic protease (Asp 2) as beta-secretase. *Mol. Cell. Neurosci.* **1999**, *14*, 419–427.
- (8) Vassar, R.; Bennett, B. D.; Babu-Khan, S.; Kahn, S.; Mendiaz, E. A.; Denis, P.; Teplow, D. B.; Ross, S.; Amarante, P.; Loeloff, R.; Luo, Y.; Fisher, S.; Fuller, J.; Edenson, S.; Lile, J.; Jarosinski, M. A.; Biere, A. L.; Curran, E.; Burgess, T.; Louis, J. C.; Collins, F.; Treanor, J.; Rogers, G.; Citron, M. Beta-secretase cleavage of Alzheimer's amyloid precursor protein by the transmembrane aspartic protease BACE. *Science* **1999**, *286*, 735–741.
- (9) Yan, R. Q.; Bienkowski, M. J.; Shuck, M. E.; Miao, H. Y.; Tory, M. C.; Pauley, A. M.; Brashler, J. R.; Stratman, N. C.; Mathews, W. R.; Buhl, A. E.; Carter, D. B.; Tomasselli, A. G.; Parodi, L. A.; Heinrichson, R. L.; Gurney, M. E. Membrane-anchored aspartyl protease with Alzheimer's disease beta-secretase activity. *Nature* **1999**, *402*, 533–537.
- (10) Sinha, S.; Anderson, J. P.; Barbour, R.; Basi, G. S.; Caccavello, R.; Davis, D.; Doan, M.; Dovey, H. F.; Frigon, N.; Hong, J.; Jacobson-Croak, K.; Jewett, N.; Keim, P.; Knops, J.; Lieberburg, I.; Power, M.; Tan, H.; Tatsuno, G.; Tung, J.; Schenk, D.; Seubert, P.; Suomensaar, S. M.; Wang, S. W.; Walker, D.; Zhao, J.; McConlogue, L.; John, V. Purification and cloning of amyloid precursor protein beta-secretase from human brain. *Nature* **1999**, *402*, 537–540.
- (11) Hardy, J. A.; Higgins, G. A. Alzheimer's disease: the amyloid cascade hypothesis. *Science* **1992**, *256*, 184–185.
- (12) Karran, E.; Mercken, M.; De Strooper, B. The amyloid cascade hypothesis for Alzheimer's disease: an appraisal for the development of therapeutics. *Nat. Rev. Drug Discovery* **2011**, *10*, 698–712.
- (13) Shimizu, H.; Tosaki, A.; Kaneko, K.; Hisano, T.; Sakurai, T.; Nukina, N. Crystal structure of an active form of BACE1, an enzyme responsible for amyloid beta protein production. *Mol. Cell. Biol.* **2008**, *28*, 3663–3671.
- (14) Xu, Y. C.; Li, M. J.; Greenblatt, H.; Chen, W. Y.; Paz, A.; Dym, O.; Peleg, Y.; Chen, T. T.; Shen, X.; He, J. H.; Jiang, H. L.; Silman, I.; Sussman, J. L. Flexibility of the flap in the active site of BACE1 as revealed by crystal structures and molecular dynamics simulations. *Acta Crystallogr., Sect. D: Biol. Crystallogr.* **2012**, *68*, 13–25.
- (15) Wang, W. R.; Liu, Y. C.; Lazarus, R. A. Allosteric inhibition of BACE1 by an exosite-binding antibody. *Curr. Opin. Struct. Biol.* **2013**, *23*, 797–805.
- (16) Ghosh, A. K.; Brindisi, M.; Tang, J. Developing beta-secretase inhibitors for treatment of Alzheimer's disease. *J. Neurochem.* **2012**, *120*, 71–83.
- (17) Ghosh, A. K.; Kumaragurubaran, N.; Tang, J. Recent developments of structure based beta-secretase inhibitors for Alzheimer's disease. *Curr. Top. Med. Chem.* **2005**, *5*, 1609–1622.
- (18) Hong, L.; Koelsch, G.; Lin, X.; Wu, S.; Terzyan, S.; Ghosh, A. K.; Zhang, X. C.; Tang, J. Structure of the protease domain of memapsin 2 (beta-secretase) complexed with inhibitor. *Science* **2000**, *290*, 150–153.
- (19) Oehrlrich, D.; Prokopcova, H.; Gijssen, H. J. The evolution of amidine-based brain penetrant BACE1 inhibitors. *Bioorg. Med. Chem. Lett.* **2014**, *24*, 2033–2045.
- (20) Baxter, E. W.; Conway, K. A.; Kennis, L.; Bischoff, F.; Mercken, M. H.; De Winter, H. L.; Reynolds, C. H.; Tounge, B. A.; Luo, C.; Scott, M. K.; Huang, Y.; Braeken, M.; Pieters, S. M. A.; Berthelot, D. J. C.; Masure, S.; Bruinzeel, W. D.; Jordan, A. D.; Parker, M. H.; Boyd, R. E.; Qu, J.; Alexander, R. S.; Brenneman, D. E.; Reitz, A. B. 2-Amino-3,4-dihydroquinazolines as inhibitors of BACE-1 (beta-site APP cleaving enzyme): Use of structure based design to convert a micromolar hit into a nanomolar lead. *J. Med. Chem.* **2007**, *50*, 4261–4264.
- (21) Tresadern, G.; Delgado, F.; Delgado, O.; Gijssen, H.; Macdonald, G. J.; Moechars, D.; Rombouts, F.; Alexander, R.; Spurlino, J.; Van Gool, M.; Vega, J. A.; Trabanco, A. A. Rational design and synthesis of aminopiperazinones as beta-secretase (BACE) inhibitors. *Bioorg. Med. Chem. Lett.* **2011**, *21*, 7255–7260.
- (22) Mateu, N.; Ciordia, M.; Delgado, O.; Sanchez-Rosello, M.; Trabanco, A. A.; Van Gool, M.; Tresadern, G.; Perez-Benito, L.; Fustero, S. A versatile approach to CF₃-containing 2-pyrrolidones by tandem michael addition-cyclization: exemplification in the synthesis of amidine class BACE1 inhibitors. *Chemistry* **2015**, *21*, 11719–11726.
- (23) Rombouts, F. J. R.; Tresadern, G.; Delgado, O.; Martínez-Lamenca, C.; Van Gool, M.; García-Molina, A.; Alonso de Diego, S. A.; Oehrlrich, D.; Prokopcova, H.; Alonso, J. M.; Austin, N.; Borghys, H.; Van Brandt, S.; Surkyn, M.; De Cleyn, M.; Vos, A.; Alexander, R.; Macdonald, G.; Moechars, D.; Gijssen, H.; Trabanco, A. A. 1,4-Oxazine β -secretase 1 (BACE1) inhibitors: from hit generation to orally bioavailable brain penetrant leads. *J. Med. Chem.* **2015**, *58*, 8216–8235.
- (24) Edwards, P. D.; Albert, J. S.; Sylvester, M.; Aharony, D.; Andisik, D.; Callaghan, O.; Campbell, J. B.; Carr, R. A.; Chessari, G.; Congreve, M.; Frederickson, M.; Folmer, R. H.; Geschwindner, S.; Koether, G.; Kolmodin, K.; Krumrine, J.; Mauder, R. C.; Murray, C. W.; Olsson, L. L.; Patel, S.; Spear, N.; Tian, G. Application of fragment-based lead generation to the discovery of novel, cyclic amidine beta-secretase inhibitors with nanomolar potency, cellular activity, and high ligand efficiency. *J. Med. Chem.* **2007**, *50*, 5912–25.
- (25) Forman, M.; Palcza, J.; Tseng, J.; Leempoels, J.; Ramael, S.; Jhee, S.; Ereshefsky, L.; Tanen, M.; Laterza, O.; Dockendorf, M.; Krishna, G.; Ma, L.; Wagner, J.; Troyer, M. The novel BACE inhibitor MK-8931 dramatically lowers cerebrospinal fluid A β peptides in healthy subjects following single- and multiple-dose administration. *Alzheimer's Dement.* **2012**, *8*, P704.
- (26) Malamas, M. S.; Erdei, J.; Gunawan, I.; Turner, J.; Hu, Y.; Wagner, E.; Fan, K.; Chopra, R.; Olland, A.; Bard, J.; Jacobsen, S.; Magolda, R. L.; Pangalos, M.; Robichaud, A. J. Design and synthesis of 5,5'-disubstituted aminohydantoin as potent and selective human beta-secretase (BACE1) inhibitors. *J. Med. Chem.* **2010**, *53*, 1146–1158.
- (27) Steele, T. G.; Hills, I. D.; Nomland, A. A.; de León, P.; Allison, T.; McGaughey, G.; Colussi, D.; Tugusheva, K.; Haugabook, S. J.; Espeseth, A. S.; Zuck, P.; Graham, S. L.; Stachel, S. J. Identification of a small molecule β -secretase inhibitor that binds without catalytic aspartate engagement. *Bioorg. Med. Chem. Lett.* **2009**, *19*, 17–20.
- (28) Bowers, S.; Xu, Y. Z.; Yuan, S.; Probst, G. D.; Hom, R. K.; Chan, W.; Konradi, A. W.; Sham, H. L.; Zhu, Y. L.; Beroza, P.; Pan, H.;

Brecht, E.; Yao, N.; Loughheed, J.; Tam, D.; Ren, Z.; Ruslim, L.; Bova, M. P.; Artis, D. R. Structure-based design of novel dihydroisoquinoline BACE-1 inhibitors that do not engage the catalytic aspartates. *Bioorg. Med. Chem. Lett.* **2013**, *23*, 2181–2186.

(29) Xu, Y. Z.; Yuan, S.; Bowers, S.; Hom, R. K.; Chan, W.; Sham, H. L.; Zhu, Y. L.; Beroza, P.; Pan, H.; Brecht, E.; Yao, N.; Loughheed, J.; Yan, J.; Tam, D.; Ren, Z.; Ruslim, L.; Bova, M. P.; Artis, D. R. Design and synthesis of thiophene dihydroisoquinolines as novel BACE1 inhibitors. *Bioorg. Med. Chem. Lett.* **2013**, *23*, 3075–3080.

(30) Ren, Z.; Tam, D.; Xu, Y. Z.; Wone, D.; Yuan, S. D.; Sham, H. L.; Cheung, H.; Regnstrom, K.; Chen, X. H.; Rudolph, D.; Jobling, M. F.; Artis, D. R.; Bova, M. P. Development of a novel beta-secretase binding assay using the AlphaScreen platform. *J. Biomol. Screening* **2013**, *18*, 695–704.

(31) Zartler, E.; Shapiro, M. *Fragment-Based Drug Discovery: a Practical Approach*; Wiley: Hoboken, 2008.

(32) Erlanson, D. A. Introduction to fragment-based drug discovery. *Top. Curr. Chem.* **2012**, *317*, 1–32.

(33) Leach, A. R.; Hann, M. M. Molecular complexity and fragment-based drug discovery: ten years on. *Curr. Opin. Chem. Biol.* **2011**, *15*, 489–496.

(34) Stamford, A.; Strickland, C. Inhibitors of BACE for treating Alzheimer's disease: a fragment-based drug discovery story. *Curr. Opin. Chem. Biol.* **2013**, *17*, 320–328.

(35) (a) De Simone, A.; Mancini, F.; Real Fernández, F.; Rovero, P.; Bertucci, C.; Andrisano, V. Surface plasmon resonance, fluorescence, and circular dichroism studies for the characterization of the binding of BACE-1 inhibitors. *Anal. Bioanal. Chem.* **2013**, *405*, 827–835. (b) In house generated K_d (SPR) and IC_{50} (FRET) values were in line with those reported by De Simone et al.

(36) Dalvit, C.; Fogliatto, G.; Stewart, A.; Veronesi, M.; Stockman, B. WaterLOGSY as a method for primary NMR screening: Practical aspects and range of applicability. *J. Biomol. NMR* **2001**, *21*, 349–359.

(37) Pervushin, K. The use of TROSY for detection and suppression of conformational exchange NMR line broadening in biological macromolecules. *J. Biomol. NMR* **2001**, *20*, 275–285.

(38) Keserü, G. M.; Erlanson, D. A.; Ferenczy, G. G.; Hann, M. M.; Murray, C. W.; Pickett, S. D. Design Principles for Fragment Libraries: Maximizing the Value of Learnings from Pharma Fragment-Based Drug Discovery (FBDD) Programs for Use in Academia. *J. Med. Chem.* **2016**, *59*, 8189–8206.

(39) Domínguez, J. L.; Christopheit, T.; Villaverde, M. C.; Gossas, T.; Otero, J. M.; Nystrom, S.; Baraznenok, V.; Lindstrom, E.; Danielson, U. H.; Sussman, F. Effect of the protonation state of the titratable residues on the inhibitor affinity to BACE-1. *Biochemistry* **2010**, *49*, 7255–7263.

(40) Pantoliano, M. W.; Petrella, E. C.; Kwasnoski, J. D.; Lobanov, V. S.; Myslik, J.; Graf, E.; Carver, T.; Asel, E.; Springer, B. A.; Lane, P.; Salemme, F. R. High-density miniaturized thermal shift assays as a general strategy for drug discovery. *J. Biomol. Screening* **2001**, *6*, 429–440.

(41) Matulis, D.; Kranz, J. K.; Salemme, F. R.; Todd, M. J. Thermodynamic stability of carbonic anhydrase: Measurements of binding affinity and stoichiometry using ThermoFluor. *Biochemistry* **2005**, *44*, 5258–5266.

(42) Fuchs, K.; Dorner-Ciossek, C.; Handschuh, S.; Heine, N.; Hoerer, S.; Klinder, K. Preparation of Substituted Amino-Benzimidazoles for the Treatment of Alzheimer's Disease. WO2009092566, 30 Jul, 2009.

(43) Vassar, R.; Kovacs, D. M.; Yan, R.; Wong, P. C. The beta-secretase enzyme BACE in health and Alzheimer's disease: regulation, cell biology, function, and therapeutic potential. *J. Neurosci.* **2009**, *29*, 12787–11794.

(44) Wang, Y. S.; Beyer, B. M.; Senior, M. M.; Wyss, D. F. Characterization of autocatalytic conversion of precursor BACE1 by heteronuclear NMR spectroscopy. *Biochemistry* **2005**, *44*, 16594–16601.

(45) Bruinzeel, W.; Yon, J.; Giovannelli, S.; Masure, S. Recombinant insect cell expression and purification of human beta-secretase (BACE-

1) for X-ray crystallography. *Protein Expression Purif.* **2002**, *26*, 139–148.

(46) VIB Protein Service Facility, UGent (PSF), UGent-VIB Research Building FSVM, Technologiepark 927, 9052 Zwijnaarde, Belgium. <http://www.dnbr.ugent.be/index.php?id=proteinservicehome> (accessed Nov 8, 2016).

(47) Centro de investigación Principe Felipe (CIPF), C/ Eduardo Primo Yúfera 3, Valencia 46012, Spain. <http://www.cipf.es/> (accessed Nov 8, 2016).

(48) Proteros GMBH, Bunsenstr. 7a, 82152 Martinsried, Germany. <http://www.proteros.com/> (accessed Nov 8, 2016).

(49) Kabsch, W. XDS. *Acta Crystallogr., Sect. D: Biol. Crystallogr.* **2010**, *66*, 125–132.

(50) Vagin, A. A.; Steiner, R. S.; Lebedev, A. A.; Potterton, L.; McNicholas, S.; Long, F.; Murshudov, G. N. REFMAC5 dictionary: organization of prior chemical knowledge and guidelines for its use. *Acta Crystallogr., Sect. D: Biol. Crystallogr.* **2004**, *60*, 2184–2295.

(51) Emsley, P.; Lohkamp, B.; Scott, W. G.; Cowtan, K. Features and development of Coot. *Acta Crystallogr., Sect. D: Biol. Crystallogr.* **2010**, *66*, 486–501.

(52) Laskowski, R. A.; MacArthur, M. W.; Moss, D. S.; Thornton, J. M. PROCHECK: a program to check the stereochemical quality of protein structures. *J. Appl. Crystallogr.* **1993**, *26*, 283–291.

(53) Beesu, M.; Malladi, S. S.; Fox, L. M.; Jones, C. D.; Dixit, A.; David, S. A. Human toll-like receptor 8-selective agonistic activities in 1-alkyl-1H-benzimidazol-2-amines. *J. Med. Chem.* **2014**, *57*, 7325–7341.

(54) Woolley, D. W.; Stewart, J. M. Synthesis of oncolytic analogs of 1,2-dimethyl-4,5-diaminobenzene. *J. Med. Chem.* **1963**, *6*, 599–601.